Luminomagnetic K2Gd1−xZr(PO4)3:Tbx3+ phosphor with intense green fluorescence and paramagnetism

ARTICLE *in* PHYSICA STATUS SOLIDI (A) APPLICATIONS AND MATERIALS · SEPTEMBER 2013

Impact Factor: 1.62 · DOI: 10.1002/pssa.201329087

4 AUTHORS, INCLUDING:

Raj Kumar
University of Rome Tor Vergata
12 PUBLICATIONS **20** CITATIONS
SEE PROFILE

Santa Chawla
National Physical Laboratory - India
92 PUBLICATIONS **789** CITATIONS
SEE PROFILE

Phys. Status Solidi A **210**, No. 9, 1933–1937 (2013) / **DOI** 10.1002/pssa.201329087

physica status solidi a
www.pss-a.com
applications and materials science

Luminomagnetic $K_2Gd_{1-x}Zr(PO_4)_3$: Tb_x^{3+} phosphor with intense green fluorescence and paramagnetism

Raj Kumar[†], Ravi Shanker[‡], Ravinder Kumar Kotnala, and Santa Chawla[*]

CSIR-National Physical Laboratory, Council of Scientific and Industrial Research, Dr. K. S. Krishnan Road, New Delhi 110 012, India

Received 1 February 2013, revised 7 May 2013, accepted 30 May 2013
Published online 5 July 2013

Keywords paramagnetism, phosphors, photoluminescence, rare earth activator

[*] Corresponding author: e-mail santa@nplindia.org, Phone: 91 11 45609242, Fax: 91 11 45609310
[†] Present address: Department of Materials for Engineering, University of Brescia, 25138 Brescia, Italy.
[‡] Present address: Department of Physics, Faculty of Engineering and Physical Sciences, University of Surrey, Guildford GU2 7XH, UK.

Multimetallic complex phosphate $K_2Gd_{1-x}Zr(PO_4)_3$:Tb_x^{3+} ($0 \leq x \leq 50$) synthesized by solid state diffusion exhibit intense green fluorescence and paramagnetic behaviour. Monophasic particles of dimensions ranging from few hundred nanometers to few micrometers could be obtained. Photo excitation at 274 nm corresponding to Gd^{3+} transition $^8S_{7/2}$–^6I_J and Gd^{3+}–Tb^{3+} charge transfer followed by emission from $^5D_{J(J=3,4)}$ to $^7F_{J(J=3,4,5,6)}$ levels of Tb^{3+} ions is observed to be the most effective photoluminescence mechanism. Paramagnetic nature was proved by VSM study. Variation of paramagnetism in undoped $K_2GdZr(PO_4)_3$ and $K_2Gd_{1-x}Zr(PO_4)_3$:Tb_x^{3+} particles and quantitative analysis by EPR indicate the role of unpaired 4f electron spin of trivalent rare earth ions in the lattice for making the particles paramagnetic.

1 Introduction Nontoxic rare earth doped fluorescent particles with magnetic properties are of recent research interest due to their potential in simultaneous fluorescence tracking and targeted drug delivery. Rare earth doped insulators comprise a class of highly efficient phosphor material in applications related to photonics, optoelectronics, lighting, and display due to their intense visible luminescence and exceptional optical damage threshold which allows them to withstand harsh conditions [1]. A host lattice comprising elements with magnetic spin and fluorescent dopant species makes a unique class of bi-functional materials with desired optical and magnetic properties. An interesting class of compounds is $K_2LnZr(PO_4)_3$ (Ln = Pr, Gd, Lu, Fe, Nd, and Y) [2, 3] of which $K_2GdZr(PO_4)_3$ (KGP) doped with Eu^{3+} in bulk material have shown quantum cutting under vacuum ultraviolet (VUV) excitation [3]. However, to the best of our knowledge, there is no report on successful synthesis; luminescence and magnetic properties of Tb doped green emitting KGP phosphor. Occurrence of magnetism in such quantum cutting phosphor material is almost [4] nonexistent. This work presents synthesis and observation of bi-functional properties such as green photoluminescence (PL) and paramagnetism in monophasic $K_2Gd_{1-x}Zr(PO_4)_3$:Tb_x^{3+} ($0 \leq x \leq 50$) particles.

2 Experimental To synthesize $K_2Gd_{1-x}Zr(PO_4)_3$:Tb_x^{3+} (KGP:Tb) with different Tb content ($0 \leq x \leq 50$), solid state diffusion reaction (SSR) was employed. The precursor components for preparing the KGP:Tb^{3+} phosphors included K_2CO_3 (99.99%); Gd_2O_3 (99.99%); $ZrOCl_2$ (99.99%); $(NH_4)_2HPO_4$ (analytical grade); Tb_4O_7 (analytical grade). All the chemicals were used without any further purification. Stoichiometric amounts of the precursors K_2CO_3, Gd_2O_3, Tb_4O_7, $ZrOCl_2$, $(NH_4)_2HPO_4$ were mixed and grind thoroughly to make fine mixture in the solid state. The fine powder was packed in recrystallized alumina boat and sintered at 1200 °C for 13 h under reducing atmosphere ($NH_3 + N_2$) in 3:1 ratio. During the sintering process, the powder was held for 13 h at peak temperature 1200 °C and then cooled down to room temperature. All the as-prepared powder samples appear white in body color. The content of Tb^{3+} was varied from 5 to 50 mol% to optimize the concentration for maximum luminescence output and the best results were obtained at

20 mol% KGP:Tb^{3+}. The sintered mass was grind thoroughly to obtain fine powder.

Structural characterization was done by XRD (Brucker-AXS D8 Advance Diffractometer) using Cu Kα radiation. Scanning electron microscope (SEM, LEO 440 system) was used to study grain morphology. PL and luminescence lifetime measurements under UV excitation were carried out using Edinburgh Instruments FLSP920 combined steady state fluorescence and phosphorescence lifetime spectrometer. Time resolved spectroscopy for luminescence lifetime measurement employed time correlated single photon counting technique using a microsecond pulsed Xe flash lamp as the source of excitation. Magnetization (M-H) of the KGP powder samples was measured at room temperature using Lakeshore 7304 vibrating sample magnetometer (VSM) using a sample holder of high purity perspex free from any metallic impurity. X-band EPR spectrometer by M/S Bruker model A 300 was used for recording EPR spectra at ambient temperature.

3 Results and discussion Synthesized $K_2Gd_{1-x}Tb_x^{3+}Zr(PO_4)_3$ samples has been indexed to the phase of $K_2GdZr(PO_4)_3$ (JCPDF No. 49-0634; Fig. 1) with the space group of $P2_13$. KGP crystallized in cubic langbeineite structure. No extra peaks for any other phase were detected indicating high solubility of Tb^{3+} in KGP in a monophase. The XRD patterns of all KGP:Tb^{3+} particles (Fig. 1) with varied Tb^{3+} concentrations indicate that as synthesized particles are crystalline without any intermediate phase, indicating that the bulk particles of multimetallic phosphate prepared by solid state diffusion process have pure crystalline phase. This is important since pure phase is favorable for luminescent properties of phosphors. The XRD peaks shift with variation in Tb concentration in $K_2Gd_{1-x}Zr(PO_4)_3:Tb_x^{3+}$ with the corresponding change in "*d*" value occurring in the third decimal place in nanometer scale. This is due to the fact that The ionic radii of Gd^{3+} (0.1078 nm) and Tb^{3+} (0.1063 nm) are very close and proper substitution would not change lattice parameters much and would cause negligible lattice strain. The morphology of the $K_2Gd_{1-x}Tb_x^{3+}Zr(PO_4)_3$ samples with different Tb concentrations were examined by scanning electron microscope (SEM) and the corresponding results are shown in Fig. 2. All K_2Gd_{1-x} $Tb_x^{3+}Zr(PO_4)_3$ samples with different concentration of Tb^{3+} exhibit separated particles of dimensions ranging from few hundred nanometers to few micrometers. The average particle size decreases with increase in Tb^{3+} concentration. According to the synthesis process employed, dense, uniform particle packing leads to an enhancement in sintering because the matter transport paths through contacts between the grains by diffusion are maximized for a minimum pore volume. SEM showed that the grains of the KGP:Tb^{3+} powder were well-defined.

The PL excitation and emission spectra of $K_2Gd_{1-x}Zr(PO_4)_3:Tb_x^{3+}$ with different concentrations of Tb^{3+} ion ($x = 5$, 10, 15, 20, 30, 40, 50 mol%) under excitation wavelength 274 nm and emission wavelength 542 nm, are presented in Figs. 3 and 4, respectively. The PL excitation and emission spectra of all the KGP:Tb samples have been measured with identical experimental parameters and normalized against sample weight. The PL excitation spectra of $K_2Gd_{1-x}Zr(PO_4)_3:Tb_x^{3+}$ show peaks at 237, 255, 274 nm corresponding to Gd^{3+} transitions $^8S_{7/2}$–^6D_J [5, 6] and $^8S_{7/2}$–^6I_J transitions [7, 8]. In the 300–328 nm band, peak at about 305, 311, 318 and a weak peak at 325 nm correspond to $^8S_{7/2}$–^6P_J transitions of Gd^{3+}. A group of f–f transitions of Tb^{3+} ion can be seen in the excitation range of 330–400 nm in the spectrum. The major peaks in the $K_2Gd_{1-x}Zr(PO_4)_3:Tb_x^{3+}$ excitation spectra indicate that there may be energy transfer from Gd^{3+} ion in the host lattice to the luminescent center Tb^{3+} ion. The energy transfer can

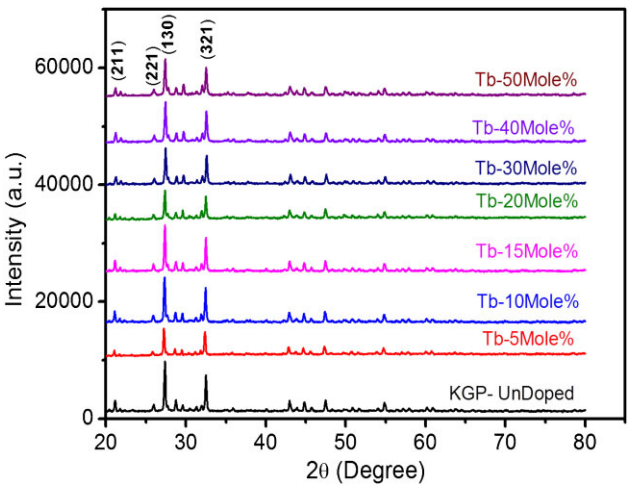

Figure 1 XRD spectrum of developed KGP and KGP:Tb^{3+} (0–50 mol%) by SSR method.

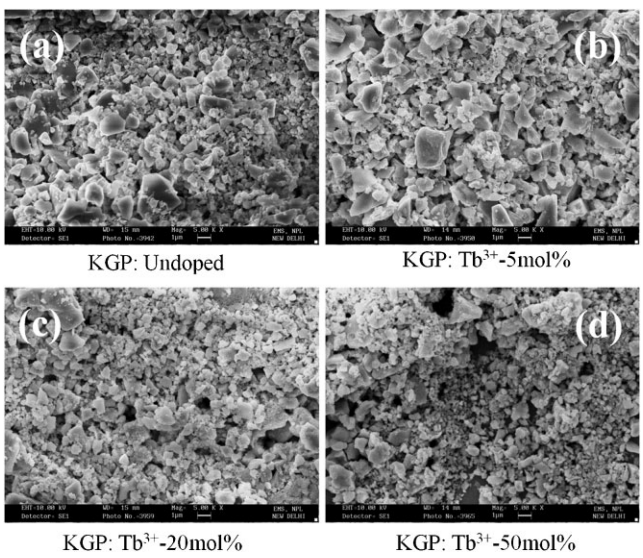

Figure 2 SEM micrograph of as synthesized (a) KGP-undoped and KGP:Tb^{3+} with Tb^{3+} concentration (b) 5 mol%, (c) 20 mol%, and (d) 50 mol%.

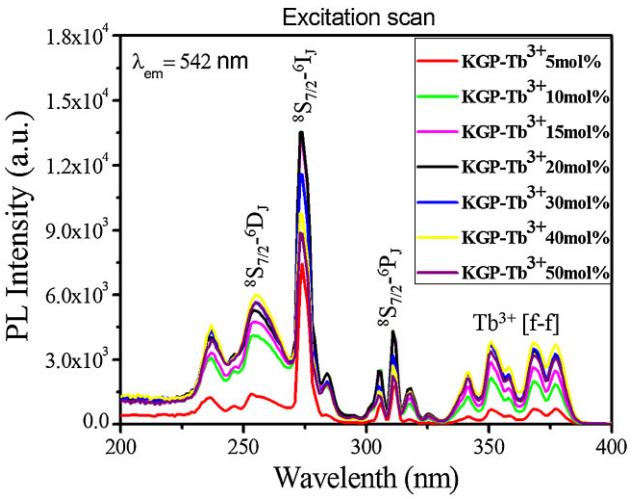

Figure 3 PL excitation spectra of KGP:Tb^{3+} at emission wavelength $\lambda_{em} = 542$ nm, for different concentrations of Tb^{3+}.

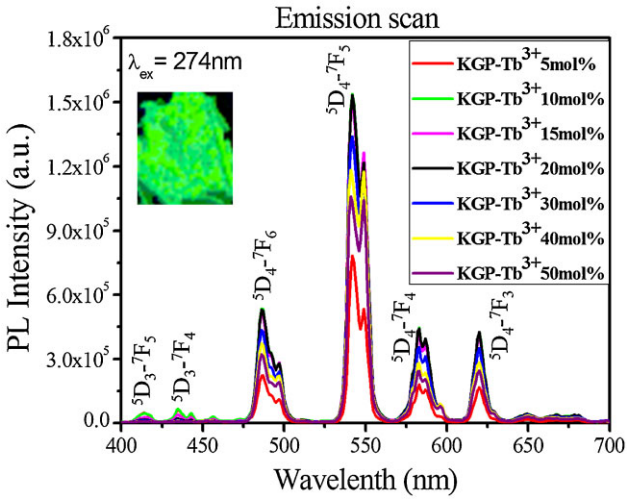

Figure 4 PL emission spectra of KGP:Tb^{3+} at $\lambda_{ex} = 274$ nm for different Tb^{3+} concentrations. The insert shows the image of the phosphor under UV excitation.

be seen by comparing the change in the intensity of excitation peaks with concentration variation of Tb^{3+} ions (Fig. 3) monitored for Tb^{3+} emission at 542 nm and is maximum for KGP:Tb^{3+} (20 mol%) particles. For lower as well as for higher concentrations of Tb^{3+}, intensity is weaker. The decrease in excitation intensity at higher concentrations could be because of concentration quenching of Tb^{3+} ion.

The PL emission spectra of KGP:Tb^{3+} under 274 nm excitation wavelength are presented in Fig. 4, the inset shows the image of the phosphor under UV excitation. The PL emission spectra of KGP:Tb^{3+} have a group of typical $^5D_4$–^7F_J ($J = 3, 4, 5, 6$) transitions of Tb^{3+}, and the highest intensity peak is the $^5D_4$–$^7F_5$ transition at 542 nm. The weak peaks at 414 and 435 nm correspond to the transitions of $^5D_3$–^7F_J ($J = 5, 4$), respectively. The intensity of PL emission peaks corresponding to $^5D_3$–^7F_J transitions decreases with increase in dopant Tb^{3+} concentration beyond 10%, because at higher concentration of Tb^{3+}, the cross relaxation produced rapid population of $^5D_4$ state at the expense of $^5D_3$, giving a strong emission in the green region. With the increase of Tb^{3+} concentration, the intensity of blue peak decreases and green peak increases. The emission peak with highest intensity is observed at 542 nm corresponding to $^5D_4$–$^7F_5$ transition of Tb^{3+} as the transition probability for both electric and magnetic dipole transition is maximum. The weaker peaks at about 583 and 619 nm correspond to $^5D_4$–$^7F_4$ and $^5D_4$–$^7F_3$ transition of Tb^{3+}, respectively [5, 9]. The low ratio of peak intensity of $^5D_3$ to $^5D_4$ peaks suggest that high phonon energy in KGP:Tb^{3+} result in phonon induced charge transfer and relaxation. In the emission spectra (Fig. 4) PL intensity is optimum at 274 nm excitation for the 20 mol% Tb^{3+} concentration in KGP microparticles with next highest PL intensity observed for the 15 mol% Tb^{3+} concentration. For the lower as well as higher concentrations of Tb^{3+}, PL intensity is weak. The strongest emission line due to $^5D_4$–$^7F_5$ transition at 542 nm, has the highest probability for both electric and magnetic dipole induced transitions and electric dipole transitions are affected by symmetry of the activator ion in the host lattice. Hence only for those Tb^{3+} concentrations (15% and 20%) when substitutional doping in Gd^{3+} site is optimum, the PL intensity is maximum. Concentration quenching sets in above 20 mol% Tb^{3+} concentration. Time resolved decay of luminescence at 542 nm emission under 274 nm excitation (Fig. 5) follows a single exponential with (1/e) decay time of 3.167 ms. Such decay times are common for $^5D_4$–$^7F_5$ transition of Tb^{3+}.

The green emitting KGP:Tb^{3+} phosphor is found to be paramagnetic as observed by continuously increasing magnetization with applied magnetic field (Fig. 6) without

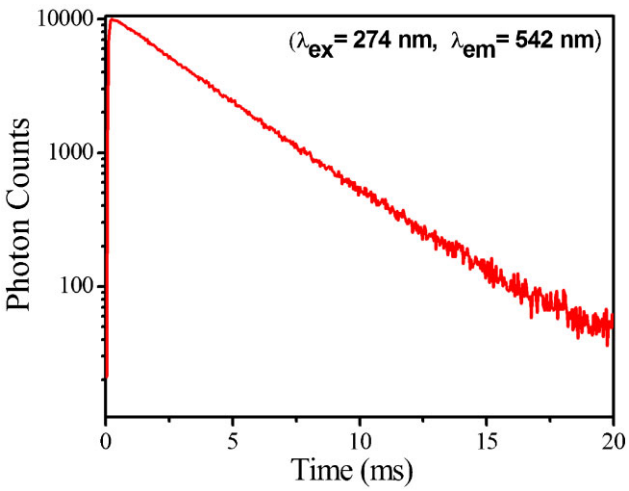

Figure 5 Time resolved decay of KGP:Tb^{3+} (20 mol%) micron size particles.

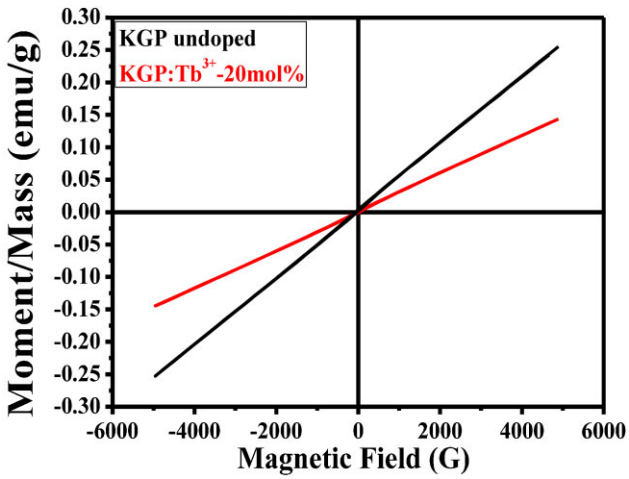

Figure 6 Magnetization curve of undoped KGP and KGP:Tb^{3+} (20 mol%) particles, exhibiting paramagnetic behavior at room temperature.

any hysteresis at room temperature with maximum magnetization of 260 and 146 memu g^{-1} at 4900 G field, for KGP and KGP:Tb (20 mol%), respectively. In order to check the origin of spin contribution, magnetic behavior of undoped KGP synthesized by identical SSR method has been investigated. KGP:Tb^{3+} exhibit less magnetization compared to undoped KGP particles as can be discerned from Fig. 6. The paramagnetic behavior of KGP arise due to strong interaction among unpaired electron spin of Gd^{3+} on 2p electrons of the neighboring oxygen which further influences the 3p orbital of phosphorous atoms. This interaction results into a long range ordered exchange force inducing paramagnetic behavior. The maximum number of unpaired 4f electrons is 7 in Gd^{3+} and KGP particles have shown magnetic behavior [10]. Moreover, spin magnetic moment of Tb^{3+} is 6/7 of the magnetic moment of Gd^{3+}. Superposition of the magnetic moments of both Gd^{3+} and Tb^{3+} could contribute towards magnetic ordering. In different langbeinite related phosphates, the spin–spin interactions between two nearest paramagnetic ions are negligible due to the structure of the compound since each nearest pair of paramagnetic atoms are connected by three atomic bridges (O–P–O) which are not very good for spin–spin interactions. Due to decrease in magnetic moment from Gd^{3+} to Tb^{3+}, the magnetization decreases with substitutional doping of Tb^3. Since Tb^{3+} ions are substituting the Gd^{3+} ions in the crystal structure, the number of Gd^{3+} ions decreases and hence magnetization has been decreased for the Tb^{3+} doped KGP as compared to undoped KGP prepared by similar SSR method (Fig. 6). As the magnetization curve shows zero coercive field and no saturation and the magnetization decreases with decrease in concentration of Gd^{3+} ions in the lattice with substitution of Tb^{3+} ions, for the $K_2GdZr(PO_4)_3:Tb^{3+}$ particles, the spin contribution from Gd^{3+} is the reason for the observed magnetic behavior [10, 11].

As EPR can probe into the paramagnetic contributors in the microsized particles and provide information about the spins and their interactions, EPR measurements were done for the same samples of undoped as synthesized KGP and KGP:Tb^{3+} particles as used for magnetic study, at constant microwave frequency of 9.5 GHz (Fig. 7). The EPR spectra exhibit one prominent line with effective g value as $g \sim 2.02$ which matches well with that reported from Gd^{3+} ions in lattice positions with strong cubic symmetry [12–15]. EPR signal intensity decreases with substitution of Tb^{3+} ions indicating decrease of spin concentration of Gd^{3+} ions due to Tb^{3+} substitution in place of Gd^{3+} ions in KGP host lattice. Further it has also been observed that the line width at half of the absorption peak of the $g = 2.02$ resonance is increased from 2537 G (KGP:Tb^{3+}) to 2883 G (KGP). The increase in line width at half of the absorption peak ($\Delta H_{1/2}$) is due to spin–spin interaction between the Gd^{3+}–Gd^{3+} ions. The spin concentrations (spin/g) have been calculated, by the comparison method using DPPH as a standard reference material, to be 3.41×10^{18} and 0.73×10^{18} spin g^{-1} for undoped KGP and KGP:Tb^{3+} particles, respectively. This clearly shows that the spin population in $K_2GdZr(PO_4)_3$ is more compared to $K_2Gd_{1-x}Zr(PO_4)_3:Tb_x$ (KGP:Tb^{3+}) particles. This is possible only when the spin contribution towards paramagnetic resonance is through Gd^{3+} ions since substitutional doping of rare earth Tb^{3+} in Gd^{3+} position reduces the effective spin concentration. Hence, EPR and magnetic measurements unambiguously point to the fact that EPR resonance and paramagnetic behavior in undoped and Tb doped KGP microparticles are due to Gd^{3+}.

High resolution magnetic force microscopy (MFM) was used to study the magnetic microstructure on pellet made of KGP:Tb^{3+} (20 mol%) phosphor particles. Figure 8a shows the surface topology investigated by atomic force microscope (AFM) and Fig. 8b the MFM image of a thin film of KGP:Tb^{3+} (20 mol%) phosphor particles. The MFM image is taken without any external magnetic field and no domain structure exist in paramagnetic material, the variation of magnetic force over an area of 5 μm × 5 μm across the

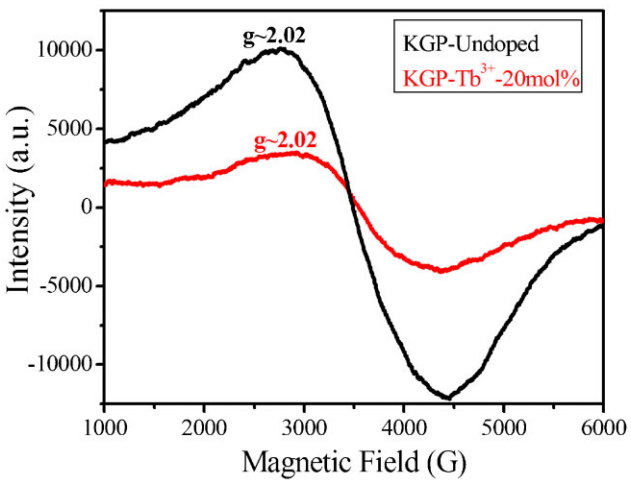

Figure 7 EPR spectra of undoped KGP and KGP:Tb^{3+} (20 mol%) bulk particles at room temperature exhibiting a broad line arising due to Gd^{3+} spins.

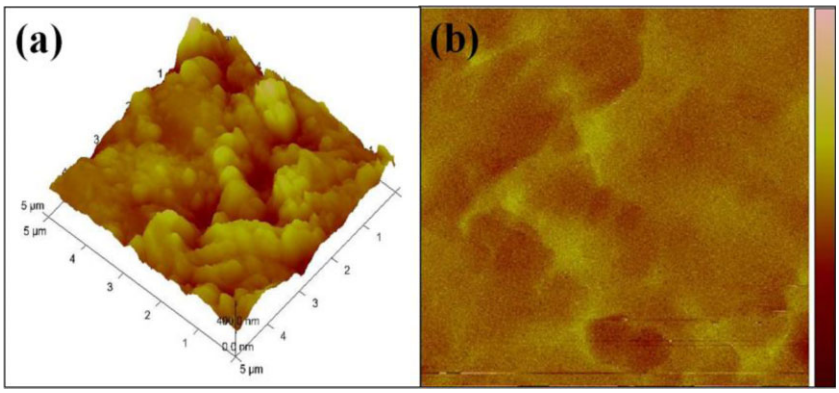

Figure 8 (a) Surface topology investigated by AFM and (b) MFM image of thin film of KGP:Tb^{3+} (20 mol%) phosphor particles.

particles is not appreciable as could be discerned from the color scale with pink indicating maximum magnetic force.

4 Conclusions Combination of bi-functional properties like strong green fluorescence emission and paramagnetic properties, make the developed KGP:Tb^{3+} phosphor suitable for applications such as display devices and in the biomedical field of medical imaging and cell tracking. The conclusive evidence of bi-functionality in KGP:Tb^{3+} particles comes from PL and magnetic (B-H) measurements that shows bright green fluorescence and continuously increasing magnetization with increase in applied magnetic field without any hysteresis.

Acknowledgement The authors (Ray Kumar, Ravi Shanker) acknowledge financial support extended by Council of Scientific and Industrial Research (CSIR), India. Authors are grateful to Mr. K.N. Sood for SEM, Dr. Manju Arora for EPR measurements.

References

[1] N. Kodama and Y. Watanabe, Appl. Phys. Lett. **84**, 4141 (2004).
[2] I. V. Ogorodnyk, I. V. Zatovsky, V. N. Baumer, N. S. Slobodyanik, and O. V. Shishkin, Cryst. Res. Technol. **1002**, 1 (2007).
[3] W. Liang and Y. Wang, Mater. Chem. Phys. **119**(1–2), 214 (2010).
[4] S. Chawla, R. Shankar, R. Kumar, A. Khan, and R. K. Kotnala, J. Lumin. **136**, 328–333 (2012).
[5] J. M. Sung, S. E. Lin, and W. C. J. Wei, J. Eur. Ceram. Soc. **27**, 2605–2611 (2007).
[6] Z.-J. Zhang, J.-L. Yuan, H.-H. Chen, X.-X. Yang, J.-T. Zhao, G.-B. Zhang, and C.-S. Shi, Solid State Sci. **11**, 549–555 (2009).
[7] C. H. Kim, I. E. Kwon, C. H. Park, Y. J. Hwang, H. S. Bae, B. Y. Yu, C. H. Pyun, and G. Y. Hong, J. Alloys Compd. **311** (1), 33–39 (2000).
[8] D. Y. Wang and N. Kodama, J. Solid State Chem. **182**(8), 2219–2224 (2009).
[9] N. Yocom, R. S. Meltzer, K. W. Jang, and M. Grimm, J. Soc. Inf. Display **4**, 169 (1996).
[10] S. Mukherjee, P. Dasgupta, and P. K. Jana, J. Phys. D **41**, 215004 (2008).
[11] G. Hadjipanayis and D. J. Sellmyer, Phys. Rev. B **23**, 3349–3354 (1981).
[12] V. Singh, R. P. S. Chakradhar, J. L. Rao, I. L. Rak, and H. Y. Kwak, J. Mater. Sci. **46**, 1038 (2011).
[13] I. V. Chepeleva, V. N. Lazukin, and S. A. Demdovskii, Sov. Phys. Dokl. **11**, 864 (1967).
[14] L. E. Iton and J. Turkevich, J. Phys Chem. **81**, 435 (1977).
[15] R. C. Nicklin, J. K. Johnstone, R. G. Barnes, and D. R. Wilder, J. Chem. Phys. **59**, 1652 (1973).